Magnetic Resonance in Medicine 51:661–667 (2004)

Inversion Recovery TrueFISP: Quantification of T_1, T_2, and Spin Density

Peter Schmitt,[1*] Mark A. Griswold,[1] Peter M. Jakob,[1] Markus Kotas,[2] Vikas Gulani,[1,3] Michael Flentje,[2] and Axel Haase[1]

A novel procedure is proposed to extract T_1, T_2, and relative spin density from the signal time course sampled with a series of TrueFISP images after spin inversion. Generally, the recovery of the magnetization during continuous TrueFISP imaging can be described in good approximation by a three parameter monoexponential function $S(t) = S_{stst}(1\text{-}INV \exp(-t/T_1^*))$. This apparent relaxation time $T_1^* \leq T_1$ depends on the flip angle as well as on both T_1 and T_2. Here, it is shown that the ratio T_1/T_2 can be directly extracted from the inversion factor *INV*, which describes the relation of the signal value extrapolated to $t = 0$ and the steady-state signal. Analytical expressions are given for the derivation of T_1, T_2, and relative spin density directly from the fit parameters. Phantom results show excellent agreement with single point reference measurements. In human volunteers T_1, T_2, and spin density maps in agreement with literature values were obtained. Magn Reson Med 51:661–667, 2004.

Key words: T_1 quantification; T_2 measurement; inversion recovery; TrueFISP; steady state free precession; SSFP

The balanced SSFP MR imaging technique (1), also named balanced FFE and FIESTA, here referred to as TrueFISP (2), was proposed more than a decade ago and has generated much renewed interest during recent years due to technical advances in gradient and receiver performance. It provides the capability of extremely rapid imaging while preserving a high SNR efficiency. With a fixed flip angle α, the steady-state signal is an increasing function of the ratio T_2/T_1, so that high signal is generally obtained from fluid compartments with a long T_2. The resulting image contrast renders the technique beneficial for several different applications, e.g., evaluation of cardiac function (3) or coronary angiography (4,5).

In practice, magnetization reaches its steady-state condition after a certain transition period. A smooth signal time course towards steady state can be achieved by preparation with an RF pulse of flip angle $-\alpha/2$, preceding the imaging sequence at a time TR/2 before the first α pulse (6). Whereas new elaborate pulse schemes have also been described (7), the $\alpha/2$-based technique is robust and allows the implementation of additional magnetization preparation experiments immediately before a TrueFISP readout. In combination with the $\alpha/2$ prepulse, an inversion recovery TrueFISP sequence has been proposed for magnetization prepared steady-state imaging (6). This approach has recently gained renewed interest as a promising tool for fast T_1 quantification (8). The intensities of a TrueFISP image series acquired after spin inversion and $\alpha/2$ preparation were reported to follow the free longitudinal relaxation curve very closely, even at comparatively high flip angles of 50°.

In a subsequent study from our group using numerical simulations and phantom experiments, it was also found that the recovery time course under a train of TrueFISP pulses can be described by monoexponential behavior (9). However, apparent relaxation times T_1^* were measured which strongly depended on the flip angle, T_1 and T_2. It was demonstrated that this property can be used to quantify both T_1 and T_2 by fitting T_1^* curves measured with different flip angles to theoretical response curves. This numerically described behavior was confirmed by the results of a recent publication wherein an elegant simplifying calculation was presented, yielding a compact mathematical description for the transient TrueFISP signal decay rate (10).

In the present work, analytical expressions are proposed for the direct calculation of T_1, T_2, and spin density from a single IR TrueFISP signal time course. Numerical simulations based on the Bloch equations were used to assess the validity of the approximations made. The feasibility and accuracy of the technique is demonstrated in phantom experiments. Results of T_1, T_2, and spin density measurements in brains of healthy human volunteers are presented.

THEORY

It was shown early that the use of matrix notation is beneficial for finding and handling solutions of the Bloch equations (11). A compact description is possible for periodic sequences, when the difference vector between an arbitrary initial value and the steady state magnetization is analyzed (7). In a recent article a subtle approximation was presented for the transient signal behavior of TrueFISP sequences, considering magnetization at zero off-resonance frequency, prepared with an initial $\alpha/2$-pulse and evolving along the $\alpha/2$-cone (10). It was shown that the temporal signal curve is expected to reveal monoexponential behavior and that a simplified expression can be obtained for the decay rate:

$$E_1^* = E_1 \cos^2\frac{\alpha}{2} + E_2 \sin^2\frac{\alpha}{2}, \qquad [1]$$

[1]Experimentelle Physik 5, Physikalisches Institut, Universität Würzburg, Germany.

[2]Klinik und Poliklinik für Strahlentherapie, Universität Würzburg, Germany.

[3]Department of Radiology, University of Michigan, Ann Arbor, Michigan, USA.

Grant sponsor: IZKF Würzburg, Project F5.

*Correspondence to: Peter Schmitt, Experimentelle Physik 5 (Biophysik), Physikalisches Institut der Universität Würzburg, Am Hubland, D-97074 Würzburg, Germany. E-mail: ps@physik.uni-wuerzburg.de

Received 9 June 2003; revised 1 December 2003; accepted 26 December 2003.

DOI 10.1002/mrm.20058
Published online in Wiley InterScience (www.interscience.wiley.com).

where α denotes the flip angle and $E_{1,2} = \exp(-TR/T_{1,2})$. For $TR \ll T_{1,2}$, this formula may be reduced to the following direct relation for an apparent relaxation time T_1^*:

$$T_1^* = \left(\frac{1}{T_1} \cos^2 \frac{\alpha}{2} + \frac{1}{T_2} \sin^2 \frac{\alpha}{2} \right)^{-1}. \quad [2]$$

With the origin of time positioned at the first imaging pulse and with T_1 relaxation between spin inversion and this pulse neglected, the TrueFISP signal value extrapolated to $t = 0$ can be described in good approximation by:

$$S_0 = M_0 \sin \frac{\alpha}{2}, \quad [3]$$

where M_0 is the proton density. The TrueFISP steady state signal may be written as (12,13):

$$S_{ststst} = \frac{M_0(1 - E_1)\sin \alpha}{1 - (E_1 - E_2)\cos \alpha - E_1 E_2}. \quad [4]$$

For $TR \ll T_{1,2}$ this expression reduces to (14):

$$S_{ststst} = \frac{M_0 \sin \alpha}{\left(\frac{T_1}{T_2} + 1\right) - \cos \alpha \cdot \left(\frac{T_1}{T_2} - 1\right)}. \quad [5]$$

Generally, the steady state signal S_{ststst} is lower than the initial signal S_0. Consequently, three parameters are needed for a complete description of the corresponding exponential IR time course from S_0 to S_{ststst}, e.g., using the fit function:

$$S(nTR) = S_{ststst}\left[1 - INV \cdot \exp\left(-\frac{nTR}{T_1^*} \right) \right]. \quad [6]$$

Here, the inversion factor *INV* indicates the ratio between S_0 and the steady state signal S_{ststst}. Using Eqs. 3 and 5, *INV* can be expressed as:

$$INV = 1 + \frac{S_0}{S_{ststst}} = 1 + \frac{\sin \frac{\alpha}{2}}{\sin \alpha} \left[\left(\frac{T_1}{T_2} + 1 \right) - \cos \alpha \left(\frac{T_1}{T_2} - 1 \right) \right]. \quad [7]$$

Thus, *INV* only depends on the flip angle and on the ratio T_1/T_2, approaching $INV = 2$ for the limit of a small flip angle. Together with Eq. 2, the following expressions are obtained so that T_1 and T_2 can be directly calculated from measured fit parameters T_1^* and *INV*:

$$T_1 = T_1^* \left[\cos^2 \frac{\alpha}{2} + (A \cdot INV + B) \sin^2 \frac{\alpha}{2} \right] \quad [8]$$

$$T_2 = T_1^* \left[\sin^2 \frac{\alpha}{2} + (A \cdot INV + B)^{-1} \cos^2 \frac{\alpha}{2} \right] \quad [9]$$

with

$$A = 2(1 - \cos \alpha)^{-1} \cos \frac{\alpha}{2} \quad [10]$$

and

$$B = \left(1 + 2 \cos \frac{\alpha}{2} + \cos \alpha \right) (\cos \alpha - 1)^{-1}. \quad [11]$$

When T_2 relaxation between the α/2-preparation and the first α-pulse is neglected, the relative spin density M_0 may be estimated directly from:

$$M_0 = \frac{S_{ststst}(INV - 1)}{\sin \frac{\alpha}{2}} \quad [12]$$

MATERIALS AND METHODS

For further analysis of the TrueFISP signal evolution during longitudinal recovery after spin inversion, numerical simulations were performed on basis of the Bloch equations using the Matlab software (MathWorks, Natick, MA). For simplification, RF pulses and signal acquisition were assumed to be infinitesimally short. IR TrueFISP experiments were modeled for various T_1, T_2, and flip angle values to assess the accuracy of the approximate equations given in the Theory section. Furthermore, simulations were used to assess the influence of off-resonance frequencies.

Experimental data were acquired on a 1.5T whole body scanner (Siemens Vision, Erlangen, Germany) using a standard quadrature head coil. A total of 18 phantom bottles with a diameter of 60 mm were examined. Fifteen bottles were filled with 0–2% agarose (Agar-Agar, Roth, Germany), doped with Gd-DTPA (Magnevist, Schering, Germany) at concentrations of 0–0.259 mmol/l. Three phantoms consisted of water doped with a SPIO contrast agent (Endorem, Guerbet, France) at concentrations of 0.025, 0.050, and 0.100 mmol(Fe)/l. With these phantoms, therefore, a wide range of T_1 and T_2 values was covered, as well as different ratios of T_2/T_1.

For reference, the longitudinal relaxation times of the phantoms were measured with a single point spin-echo (SE) sequence. After adiabatic inversion, spoiling of residual transverse magnetization and subsequent delay TI, a single line of *k*-space was acquired, followed by a delay of 15 sec before the next inversion. Images were acquired at 14 different inversion times, ranging from TI = 25 ms to TI = 9 sec. Transverse relaxation was assessed with a CPMG-sequence. After 90°-excitation, a total of 16 echoes with an interecho distance of 50 ms were acquired. To minimize T_1 influence, a long TR of 10 sec was used. Reference values for T_{1ref} and T_{2ref} were calculated from the corresponding magnitude image series by three-parameter and two-parameter fitting routines, respectively.

IR-TrueFISP experiments were performed on the phantoms arranged in groups, at flip angles between 10° and 130° with a segmented imaging sequence (TR = 6.46 ms, bandwidth = 488 Hz/pixel). After adiabatic inversion, a train of 38 image segments was acquired. Each segment was comprised of 21 phase-encoding steps, equally dis-

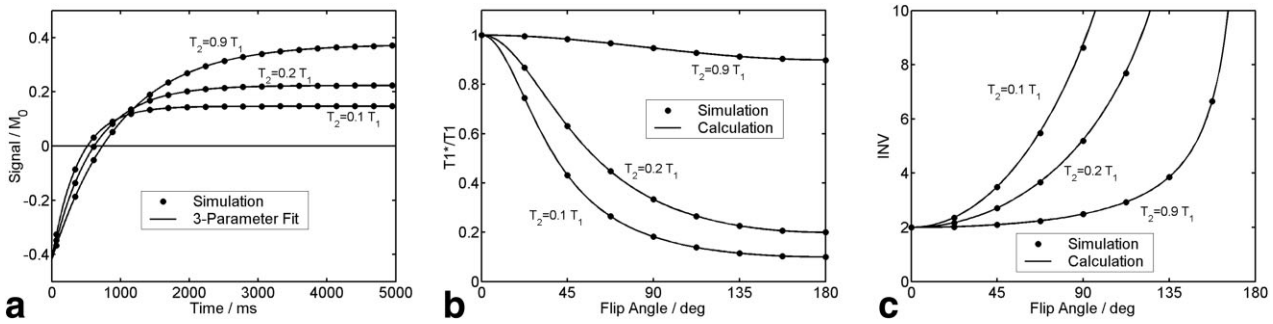

FIG. 1. Simulations and calculations: (**a**) signal time courses with a flip angle of 50° for different ratios T_2/T_1; (**b**) ratio of apparent T_1^* to true T_1; and (**c**) inversion factor *INV* over the flip angle.

tributed over *k*-space with spacings of 12 steps. Thus, the recovery curve was sampled for more than 5 sec. A delay of 5 sec was introduced to allow for longitudinal relaxation before the next inversion. A square field of view of 256 mm was covered with a matrix of 252 × 256 pixels, yielding a total time of 2:08 min for the complete acquisition of 38 images. A sinc-shaped RF pulse was used, which had been optimized for a rectangular slice profile with thickness 8 mm. The same sequence was used for parameter measurements in the human brain. Healthy volunteers were examined after giving informed consent. After shimming, IR TrueFISP image series were acquired with different flip angles in axial slices. For later comparison, T_1-, T_2-, and spin density-weighted MR images were acquired in the same slice positions with an SE sequence (TE = 14 ms, TR = 500 ms) and with a dual contrast turbo-spin-echo (TSE) sequence (TE_{eff} = 16/98 ms, TR = 4000 ms).

The acquired IR TrueFISP magnitude image series were fit pixelwise to the three-parameter function given in Eq. 6 using a least-square fitting routine and a computing algorithm described in Ref. 15. From the resulting fit parameter maps, T_1, T_2, and M_0 maps were calculated using Eqs. 8–12.

In the phantom data, values were taken from regions of interest (ROIs) placed within the bottles and compared to the corresponding results obtained in the same manner from SE and CPMG sequences. In the in vivo data, T_1, T_2, and M_0 values were evaluated in ROIs positioned in white matter, gray matter, cerebrospinal fluid (CSF), and muscle tissue, each ROI comprising at least 25 pixels. From the parameter maps, synthetic T_1-, T_2-, and spin density-weighted images were calculated and compared to the corresponding acquired SE and TSE images by means of a pixel-based correlation.

RESULTS

For magnetization at zero or small off-resonance frequency, the simulated temporal signal curves revealed essentially pure monoexponential behavior and could thus be completely characterized by three fit parameters: T_1^*, S_{stst}, and *INV*. This is demonstrated in Fig. 1a, where three temporal signal courses, simulated for a flip angle of 50° and different ratios of T_2/T_1, are depicted together with the corresponding monoexponential fits. In Fig. 1b,c, results for T_1^* and *INV* are shown for different T_2 values as a function of the flip angle, obtained with numerical simulations and analytic calculations according to Eqs. 2 and 7. The value of T_1^* equals the true T_1 at small flip angles and approaches T_2 in the multispin-echo limit of $\alpha = 180°$ (Fig. 1b). *INV* equals 2 at small flip angles and is even close to 2 for higher flip angles, when $T_2 \approx T_1$. Both T_1^* and *INV* as calculated from Eqs. 2 and 7 correspond to the results from Bloch simulations very closely (Fig. 1c). For brain tissue (e.g., white matter with T_1 = 700 and T_2 = 75), a short T_1^* of ~287 ms and an inversion factor of *INV* = 3.63 would be expected with a flip angle of 50°.

For spins not on resonance, more and more distinctive initial signal oscillations are observed as well as a subtle persistent deviation from the respective on-resonant time course. The signal curves still fit well to monoexponential functions but errors are introduced in the calculation of T_1, T_2, and M_0 values. This is illustrated in Fig. 2, where the parameter values determined at different flip angles are plotted against the off-resonance angle, i.e., the dephasing angle during the TR interval. For the depicted simulations, a T_1 of 1000 ms and a T_2 of 100 ms were used, but the relative deviations from the true values were largely independent of T_1 or of the ratio T_2/T_1, i.e., the depicted results represent estimates for various tissues. For example, with a flip angle of 50° and at an off-resonance angle of $\pi/3$, which corresponds to a frequency offset of 26 Hz for the TR of 6.46 ms used here, T_1 and M_0 are overestimated by less than 4% and by roughly 12%, respectively, while the measured T_2 values are about 20% too high. However, off-resonance appeared not to be a problem in our studies on phantoms and the human brain.

In the phantom experiments, the single pixel signal courses were well characterized by the monoexponential three-parameter fit function according to Eq. 6. The complete T_1, T_2, and M_0 parameter maps obtained with a flip angle of 50° are shown in Fig. 3a–c. The gray scales of the T_1 and T_2 map were truncated at 3500 ms and 1400 ms, respectively. The spin density values were normalized to the average value of all phantoms, indicated in arbitrary units. In some phantoms, thin fluid films have formed between the agar matrix and the bottle wall. In the T_2 map they appear as bright rings at the phantom rims, corresponding to long T_2 values. They are not visible in the T_1 map, since T_1 is mainly determined by the Gd concentration, which can be expected to be essentially identical for the agar gel and the surrounding fluid. Rather similar M_0

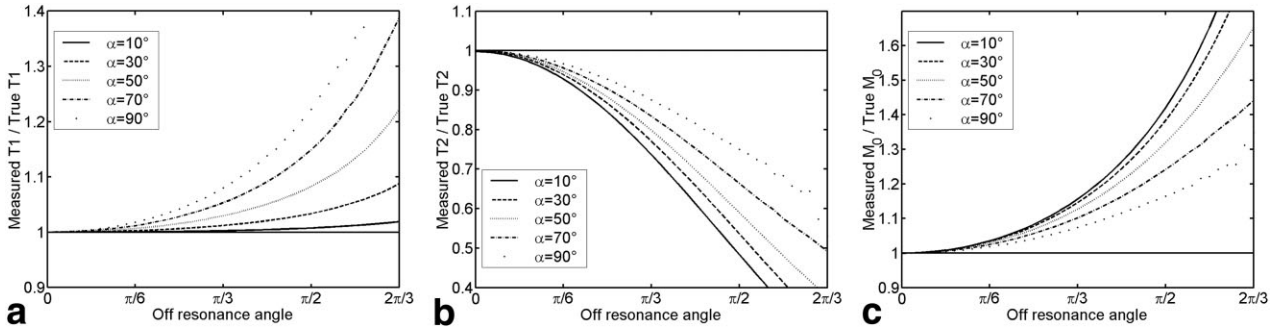

FIG. 2. Simulated influence of off-resonance frequency: ratio of measured parameter value to true value at flip angles from 10° to 90° over the off-resonance angle: (**a**) T_1 (**b**) T_2 (**c**) M_0.

values are observed in the differently doped bottles, which is expected since spin density should not show strong dependence on the concentration of contrast agent or agarose.

An overview of all phantom results at $\alpha = 50°$ is given in Fig. 3d–f. Here, the T_1, T_2, and M_0 values measured with the TrueFISP sequence are plotted vs. the corresponding reference values. The excellent agreement with the single point values for all phantoms covering wide ranges of T_1 and T_2 is apparent in the high correlation coefficients of $r^2 = 0.999$ and $r^2 = 0.996$ for the T_1 and T_2 data and in the clustering of all M_0 values near to 1, as expected. Equivalent results were obtained with flip angles between 30° and 90°. With a smaller flip angle of 10°, the measured T_1^* values were similar to the calculated T_1 and the reference T_1 values. However, the obtained T_2 and M_0 maps had a noisy appearance and the reference values were not reproduced precisely (data not shown). With flip angles higher than 90°, short T_1^* values and limited accuracy for the determination of all parameters were observed.

In the in vivo study, a similar impact of the choice of the flip angle was observed. Accurate measurements were shown to be feasible at flip angles between 30° and 70°. A low flip angle of 10° resulted in noisy T_2 maps and high flip angles of 90° and above lead to very short T_1^* values which could not be recorded precisely. In Fig. 4, representative in vivo results of a volunteer brain are shown, measured with an IR TrueFISP experiment at a flip angle of 50°. The calculated T_1, T_2, and spin density parameter maps are depicted in Fig. 4a–c. For better visualization, the gray scales of the relaxation time maps were truncated at 3500 ms and 250 ms, respectively. The spin density map was normalized to $M_0 = 1$ for the maximum value found in CSF. In Table 1, average parameter results are given, obtained within ROIs positioned in gray matter, white matter, CSF, and muscle tissue. With the exception of a comparatively low spin density of CSF, the measured values fit well into the range of literature values and were be reproducible in the same subject. Similar results were obtained in all volunteers.

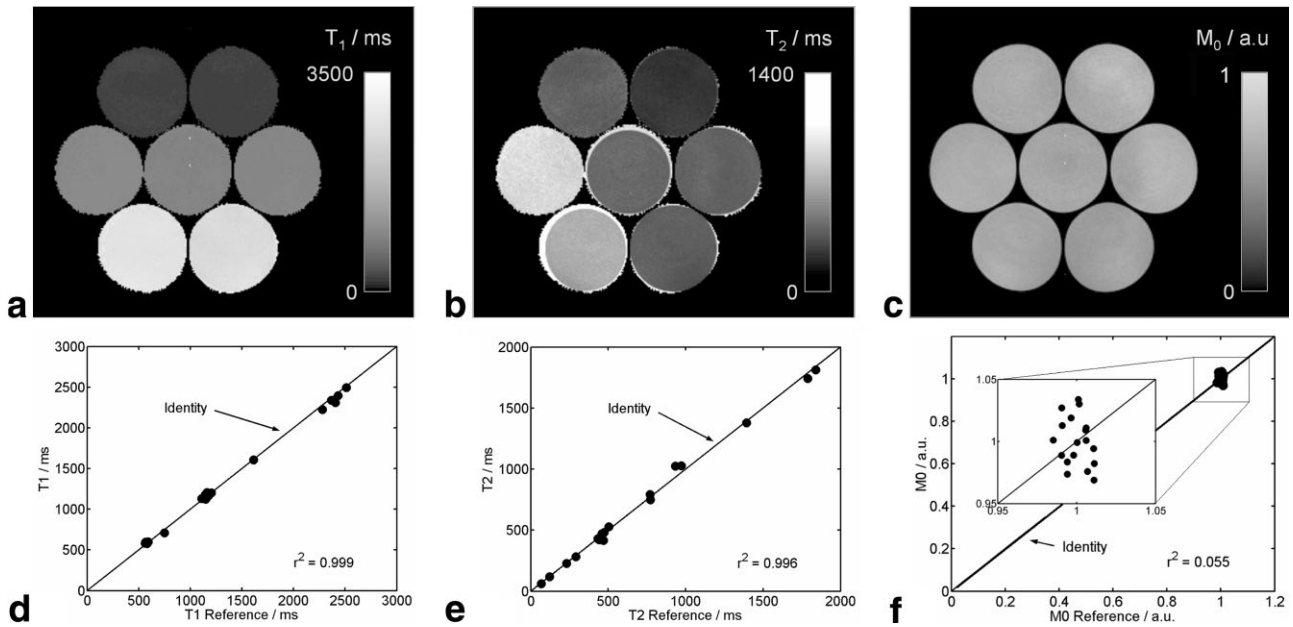

FIG. 3. Phantom results: (**a**) T_1, (**b**) T_2, and (**c**) spin density map of grouped phantoms. (**d**) T_1 and (**e**) T_2 and (**f**) spin density of all phantoms over the corresponding reference values.

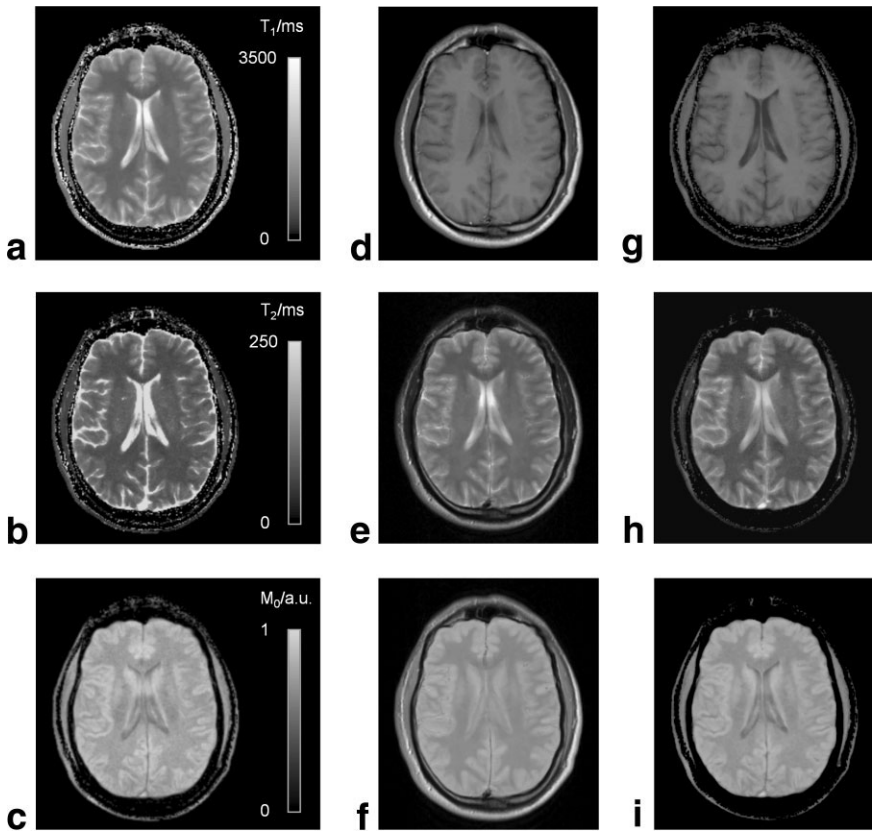

FIG. 4. Volunteer data: parameter maps measured with a IR TrueFISP experiment at a flip angle of 50°: (**a**) T_1, (**b**) T_2, and (**c**) spin density. Comparison between synthetic and acquired images: (**d**) T_1-weighted SE (TE = 14 ms, TR = 500 ms), (**e**) T_2-weighted TSE (TE_{eff} = 98 ms, TR = 4000 ms), (**f**) spin density-weighted TSE (TE_{eff} = 16 ms, TR = 4000 ms), (**g–i**) corresponding images computed from the parameter maps.

In Fig. 4d–f, T_1-, T_2-, and spin density-weighted MR images are depicted that were acquired with the SE and TSE sequences. The corresponding synthetic images calculated from the parameter maps are shown in Fig. 4g–i, respectively. They essentially show the same contrast behavior as the original images, except in voxels with high in-plane flow, as in the sagittal sinus, in regions containing fat or CSF, and in those voxels affected by partial volume effects, primarily at tissue interfaces outside the skull. This visual finding is confirmed by the high correlation coefficients of $r = 0.83$, $r = 0.89$, and $r = 0.73$ between computed T_1-, T_2-, and spin density-weighted images, respectively, and their acquired counterparts which were calculated from all pixels within a ROI encompassing the whole brain. Even higher r values are obtained when the ventricles are omitted from the ROI.

DISCUSSION

The idea of acquiring a series of TrueFISP images after spin inversion had been proposed early on for T_1-prepared steady-state imaging (6). From a later study on phantoms doped with Gd-DTPA, it was reported that the measured IR TrueFISP time course with a flip angle of 50° reflected free longitudinal relaxation very closely (8). However, in Gd-doped phantoms, T_2 is close to T_1, so that the apparent TrueFISP T_1^* may be equal to the true T_1 for purely coincidental reasons. In most biological tissues, T_2 is substantially shorter than T_1. Thus, an apparent relaxation constant T_1^* is expected that is much shorter than the real T_1, with its value also depending on the flip angle. When the complete recovery time course information is incorporated, e.g., using a three-parameter fit according to Eq. 6, it is possible to extract both T_1 and T_2 as well as relative spin density. Both our phantom and in vivo results confirm the feasibility and accuracy of the technique.

Table 1
Volunteer Data: Parameter Values Obtained from ROIs Positioned in Different Tissues (Mean ± SD)

	T_1/ms	T_2/ms	M_0/a.u.
White matter	719 ± 33	73 ± 6	0.81 ± 0.03
Gray matter	1165 ± 88	92 ± 11	0.98 ± 0.07
CSF	3337 ± 111	2562 ± 123	1.00 ± 0.07
Muscle	963 ± 78	60 ± 12	0.79 ± 0.05

Although several simplifying assumptions underlie the proposed calculations, the results correspond very closely to those of numerical Bloch simulations. These still cannot reflect real experimental conditions, since, for example, the duration or potential inaccuracies of RF pulses and signal reception are not accounted for. In vivo, blood or CSF flow into the imaging slice may affect the results. These were not considered, nor were diffusion effects which may generally influence the signal in TrueFISP imaging (16).

A direct comparison of quantitative relaxation constants with the literature is difficult, as various values for T_1 and T_2 of brain parenchyma are reported from previous studies. While both lower and higher values can be found, most reported T_1 values of white matter lie between 633 ms and 758 ms, while those of cortical gray matter

range between 998 ms and 1304 ms (17–21). Whereas transverse relaxation in the brain may be characterized best with a multiexponential decay (22), a reasonable range of T_2 values for a monoexponential model is 69 ms to 81.1 ms in white and 77.9 ms to 93.3 ms in gray matter (17,18,20,22). Our values given in Table 1 are in close agreement with these reports from the literature. The spin density ratio between gray and white matter determined here is very close to previously reported values between 0.84 and 0.88 (18,23,24). Reasonable results were obtained in muscle and CSF, except spin density values of CSF, which may be underestimated due to incomplete relaxation during the 5-sec waiting periods before the subsequent inversion pulses. These findings are confirmed by the good correlation between real SE or TSE images and synthetic images calculated from parameter maps, in particular given that experiments with completely different slice profiles are compared and that the match may be hampered by potential motion between the multiple scans.

An important point to discuss is the sensitivity of TrueFISP to off-resonance. The typical banding artifacts can be avoided when the off-resonance dephasing angle during TR is less than $\pm\pi$, a condition that could easily be fulfilled over a phantom group or over a human brain, even for the moderate TR of 6.46 ms. Furthermore, the theoretical approximation used for data evaluation is only valid for on-resonant spins. With Bloch simulations, it was possible to demonstrate the sensitivity of the technique to off-resonance. In particular, for magnetization at frequencies considerably off-resonance, the sequence preparation with the preceding $\alpha/2$ pulse would not be perfect. Oscillations in the first echoes would be expected, inevitably associated with image artifacts, particularly in our case of segmented acquisition. However, in our experience artifacts were not encountered, not even in the first image after inversion, which is acquired with only the first 21 echoes after preparation. Consequently, it may be assumed that serious problems with off-resonant magnetization did not occur. Both our phantom and volunteer studies demonstrate the feasibility of the technique and that it is possible to measure three different parameters with a single IR TrueFISP experiment.

With a low flip angle of 10°, an apparent T_1^* was obtained that is close to the real T_1. This is due to the fact that in that case the magnetization vector remains essentially parallel to the main magnetic field, and therefore predominantly follows longitudinal relaxation. Consequently, the component of the magnetization vector which is subjected to transverse relaxation and the resulting influence of T_2 on the signal time course are too small for precise quantification of T_2. With a larger flip angle, e.g., 70°, the transverse magnetization component, and thus the precision of measuring transverse relaxation, is increased. On the other hand, the steady-state signal may be maximal for flip angles of only 30° in brain tissue, suggesting that the chosen flip angle should not be chosen too large. In addition, the apparent relaxation time decreases for increasing flip angle. At a flip angle of 90°, a T_1^* of only 138 ms is expected for white matter (T_1 = 700 ms, T_2 = 75 ms), which is in the range of the temporal distance between two consecutive images in our study. In this case, the temporal resolution used here proved to be too small for precise sampling of the signal recovery curve. At high flip angles, the images would have to be divided into smaller segments and, consequently, the total scan time would be increased. For these reasons the optimum excitation angle as well as the best segmentation scheme for this angle will depend on the expected T_1 and T_2 values. The question is not trivial and should be the subject of further investigations.

For the presented data evaluation, the inversion factor *INV* has to be measured precisely. For an accurate fit of the steady-state signal value, the recovery curve should ideally be sampled at least until the steady-state condition is reached. In our study, the signal time course was observed for more than 5 sec, by far long enough to reach the steady state in brain tissue, but too short for CSF. Thus, if the focus is on parenchyma only, the recovery sampling time could be substantially shortened, also leading to shorter total scan times. For optimized measurements in CSF, it may be beneficial to acquire more images. Furthermore, any loss of longitudinal magnetization due to incomplete recovery before inversion or an imperfect inversion pulse will lead to errors. With the use of an adiabatic hyperbolic secant inversion pulse the second influencing factor may be minimized, at least when a coil with homogeneous B_1 field is used. However, for complete recovery, a long delay is required before inversion. The delay of 5 sec used in our experiments was shown to be sufficiently long to give reasonable results for gray and white matter, but errors may be introduced for the results in voxels with long T_1, such as CSF.

With a saturation recovery sequence, no delay would be required and the total scan time could be significantly reduced. However, additional information would be necessary to obtain a unique solution of T_1 and T_2. This may be accomplished with two experiments at different flip angles and a postprocessing procedure similar to that proposed previously (9). Whether this approach is beneficial for the efficiency of T_1 and T_2 quantification has yet to be determined.

The TR of the TrueFISP sequence used in our studies was 6.46 ms, which is quite moderate compared to the short TRs under 3 ms which are available on newer clinical scanners. However, it was possible to use a long RF pulse which could thus be optimized for slice profile effects. With a shorter TR, potential influence of off-resonance effects is minimized and a higher temporal SNR efficiency may be achievable. On the other hand, very short RF pulses have to be used which leads to an inevitably poor slice profile. With a broad flip angle distribution over the slice, the complex integral over different recovery curves will be measured, each with its own apparent relaxation constant. This will lead to a more complicated recovery curve, which will probably not be described adequately by a monoexponential function. However, the flip angle distribution along the slice profile can easily be measured and this information may also be included into the theory. This problem may be avoided with a 3D sequence.

CONCLUSIONS

Our results show that it is possible to derive both T_1 and T_2 as well as relative spin density from a single IR TrueFISP

experiment. The optimization of all sequence parameters and a thorough comparison with conventional techniques regarding SNR, T_1, and T_2 accuracy should be the subject of further research. No problems with off-resonance and imperfect pulse profiles occurred in this study, but the robustness of the technique with respect to these effects has to be explored.

REFERENCES

1. Oppelt A, Graumann R, Barfuss H, Fischer H, Hartl W, Schajor W. FISP — a new fast MRI sequence. Electromedica 1986;54:15–18.
2. Haacke EM, Wielopolski PA, Tkach JA, Modic MT. Steady-state free precession imaging in the presence of motion: application for improved visualization of the cerebrospinal fluid. Radiology 1990;175:545–552.
3. Lee VS, Resnick D, Bundy JM, Simonetti OP, Lee P, Weinreb JC. Cardiac function: MR evaluation in one breath hold with real-time true fast imaging with steady-state precession. Radiology 2002;222:835–842.
4. Carr JC, Simonetti O, Bundy J, Li D, Pereles S, Finn JP. Cine MR angiography of the heart with segmented true fast imaging with steady-state precession. Radiology 2001;219:828–834.
5. Spuentrup E, Bornert P, Botnar RM, Groen JP, Manning WJ, Stuber M. Navigator-gated free-breathing three-dimensional balanced fast field echo (TrueFISP) coronary magnetic resonance angiography. Invest Radiol 2002;37:637–642.
6. Deimling M, Heid O. Magnetization prepared true FISP imaging. In: Proc 2nd Annual Meeting ISMRM, San Francisco, 1994.
7. Hargreaves BA, Vasanawala SS, Pauly JM, Nishimura DG. Characterization and reduction of the transient response in steady-state MR imaging. Magn Reson Med 2001;46:149–158.
8. Scheffler K, Hennig J. T1 quantification with inversion recovery TrueFISP. Magn Reson Med 2001;45:720–723.
9. Schmitt P, Griswold M, Fidler F, Jakob PM, Kotas M, Flentje M, Haase A. Quantification of both T1 and T2 values with IR TrueFISP experiments. In: Proc 19th Annual Meeting of the ESMRMB, Cannes, France, 2002. #469.
10. Scheffler K. On the transient phase of balanced SSFP sequences. Magn Reson Med 2003;49:781–783.
11. Jaynes ET. Matrix treatment of nuclear induction. Phys Rev 1955;98: 1099:1105.
12. Freeman R, Hill HDW. Phase and intensity anomalies in Fourier transform NMR. J Magn Reson 1971;4:366–383.
13. Zur Y, Stokar S, Bendel P. An analysis of fast imaging sequences with steady-state transverse magnetization refocusing. Magn Reson Med 1988;6:175–193.
14. Haacke EM, Brown RW, Thompson MR, Venkatesan R. Magnetic resonance imaging: physical principles and sequence design. Chap. 18. St. Louis: Mosby; 1999.
15. Nekolla S, Gneiting T, Syha J, Deichmann R, Haase A. T1 maps by k-space reduced snapshot-FLASH MRI. J Comput Assist Tomogr 1992; 16:327–332.
16. Buxton RB. The diffusion sensitivity of fast steady-state free precession imaging. Magn Reson Med 1993;29:235–243.
17. Breger RK, Rimm AA, Fischer ME, Papke RA, Haughton VM. T1 and T2 measurements on a 1.5-T commercial MR imager. Radiology 1989;171: 273–276.
18. Whittall KP, MacKay AL, Graeb DA, Nugent RA, Li DK, Paty DW. In vivo measurement of T2 distributions and water contents in normal human brain. Magn Reson Med 1997;37:34–43.
19. Henderson E, McKinnon G, Lee TY, Rutt BK. A fast 3D Look-Locker method for volumetric T1 mapping. Magn Reson Imag 1999;17:1163–1171.
20. Vymazal J, Righini A, Brooks RA, Canesi M, Mariani C, Leonardi M, Pezzoli G. T1 and T2 in the brain of healthy subjects, patients with Parkinson disease, and patients with multiple system atrophy: relation to iron content. Radiology 1999;211:489–495.
21. Srinivasan R, Henry R, Pelletier D, Nelson S. Standardized, reproducible, high resolution global measurements of T1 relaxation metrics in cases of multiple sclerosis. AJNR Am J Neuroradiol 2003;24:58–67.
22. Poon CS, Henkelman RM. Practical T2 quantitation for clinical applications. J Magn Reson Imag 1992;2:541–553.
23. Brix G, Schad L Lorenz W. Evaluation of proton density by magnetic resonance imaging: phantom experiments and analysis of multiple component proton transverse relaxation. Phys Med Biol 1990;35:53–66.
24. Roberts DA, Rizi R, Lenkinski RE, Leigh JS Jr. Magnetic resonance imaging of the brain: blood partition coefficient for water: application to spin-tagging measurement of perfusion. J Magn Reson Imag 1996;6: 363–366.